



Search for ZW/ZZ Production in Leptons + Jets channel

The CDF Collaboration
URL <http://www-cdf.fnal.gov>
(Dated: July 21, 2011)

We present the results of studies aimed at an experimental measurement of WZ/ZZ diboson production in the dilepton + dijet final state using 6.6 fb^{-1} of data recorded with the CDF detector at the Fermilab Tevatron collider. We select events by identifying those that contain two charged leptons with a reconstructed invariant mass near the mass of the Z boson, two hadronic jets, and low transverse missing energy. We introduce a new quark-gluon neural network discriminant that quantizes the spatial spread of the energy and track momenta contained within a jet. We use this variable to correct our background modeling for differing jet energy scales for gluon-like and quark-like jets. We attempt to extract our signal through a fit to the dijet mass spectrum in three channels: a heavy-flavor tagged channel, a light-flavor tagged channel, and an untagged channel. We do not see a significant presence of signal, and present a limit on the measured cross section of $1.3 \times \sigma_{WZ+ZZ} = 6.6 \text{ pb}$ at 95% CL, compared to the expected limit of $2.3 \times \sigma_{WZ+ZZ}$.

I. INTRODUCTION

Experiments at the Tevatron have measured the production of two gauge bosons in both entirely leptonic decay channels and, recently, in partially hadronic decay channels[1, 2]. Measurements of diboson production are difficult to carry out due to the very small production cross sections of these processes, on the order of 10 pb or less. Furthermore, analyses in each decay channel encounter extra difficulties: leptonic decay channels present relatively clean signals, but face issues with low branching ratios for gauge boson decays; on the other hand, partially hadronic decay channels have higher expected event yields, but also much higher expected backgrounds from QCD multi-jet processes and $Z/W + \text{jets}$ events.

While the search for a very rare Standard Model process is exciting enough, analyses of diboson production are even more motivated by their close relationship to searches for the Higgs boson. If the Higgs boson is above $140 \text{ GeV}/c^2$ in mass, its most likely decay channel will be to two W bosons, with detector signatures similar to WW production. If the Higgs is lighter, it will more likely decay to a $b\bar{b}$ pair. In this scenario, the best chance for an observation of the Higgs will be in the associated production of a Higgs boson with an electroweak gauge boson (WH or ZH). Thus, partially hadronic decay channels of diboson production will have a similar signature to associated Higgs production, as one boson decays leptonically, and the other (a W or Z in the diboson production case, and the Higgs in associated production) hadronically.

In this note, we present our work towards the measurement of the cross section of ZZ and ZW production at CDF, where a Z boson decays to either electrons or muons, and the other boson decays to quarks (due to the energy resolution of our calorimeter, we are unable to distinguish between quarks coming from a W or Z boson, so we consider both). While this channel has the benefit of little QCD multi-jet background, it suffers from a very significant Z + jets background, and a rather small number of events due to the small branching ratio of Z decays to charged leptons.

To extract our signal, we fit the dijet mass spectrum in a $Z + 2 \text{ jets}$ selection region with expected background and signal shapes from Monte Carlo simulations to obtain a measurement of the signal cross section. We make use of a new NN quark-gluon discriminant to try to separate out our signal (quark-jets from the decays of massive bosons) from the dominant $Z + \text{jets}$ background, while also making use of the NN-based jet bness tagger, described in [2], to separate out Z decays to heavy flavor quarks.

II. DATA SELECTION, BACKGROUNDS AND DATA SETS

The final state we are searching for includes two charged leptons from the decay of a Z boson, and two jets from the decay of a W or Z boson. For our leptonic Z, we select events with an electron-positron or muon-antimuon pair which pass our high- p_T electron and muon triggers. We require each lepton $p_T > 20 \text{ GeV}/c$, in order to satisfy the trigger requirement, and the reconstructed Z boson mass to be between $76 \text{ GeV}/c^2$ and $106 \text{ GeV}/c^2$. Additionally, we require the reconstructed $ZP_T > 10 \text{ GeV}/c$, and that there is little transverse momentum imbalance ($\cancel{E}_T < 25 \text{ GeV}$). The former cut improves the modeling of our data, while the latter cut removes contributions from $t\bar{t}$ events.

We require jets selected for our analysis to have $E_T > 20 \text{ GeV}$ (using energy corrections meant to match the original parton energy), $|\eta| < 2.0$, and jet EM fraction > 0.9 . For all jets in MC simulation matched to gluons, we lower the jet energy scale by 2σ , as will be described in Section IV.

We use a $Z + 0 \text{ jet}$ selection region to calibrate the modeling of the energies of our electrons, adjusting the energy in our MC to match the peak at the Z boson mass observed in data. We determine the trigger efficiency and lepton identification reconstruction efficiencies by comparing data and Monte Carlo simulation in a $Z + 1 \text{ jet}$ selection. We require that in our signal region, with $Z + 2$ or more jets, that the ΔR between the two leading jets be greater than 0.75, in order to improve the modeling of the dijet mass. The cuts we make for our Z selection are summarized in Table I.

After this selection, we have four major classes of backgrounds.

1. Electroweak (EWK): Z boson+jets processes that pass our selection requirements. They are estimated using Monte Carlo calculations.
2. Fakes: Events where we have one real lepton and one lepton faked by a jet. We use a data-driven estimate for these backgrounds, using same-sign dilepton events to estimate muon fakes, and using electron-jet pairs to model electron fakes. The latter is assigned a fake rate dependent on the E_T and η of the jet, derived from jet-triggered data.
3. Top quark pair production, where we have $t\bar{t} \rightarrow l\nu l\nu b\bar{b}$. We estimate this background using a Monte Carlo calculation.

Event Selection Requirements
Inclusive Z
$N_{vtx} > 0$ $ z_0 < 60$ cm 1 st /2 nd lepton $P_T > 20$ GeV/ c Δz_0 between leptons < 5 cm (for central electrons and muons) $76 \text{ GeV}/c^2 < M_{ll} < 106 \text{ GeV}/c^2$ $\cancel{E}_T < 25$ GeV
$Z + 1$ jet
All inclusive Z requirements above Reconstructed $Z P_T > 10$ GeV/ c N_{jets} with $E_T > 20$ GeV = 1 Jet $E_T > 20$ GeV, $ \eta < 2.0$
$Z + 2$ jet (signal region)
All inclusive Z requirements above Reconstructed $Z P_T > 10$ GeV/ c N_{jets} with $E_T > 20$ GeV ≥ 2 1 st /2 nd jet $E_T > 20$ GeV, $ \eta < 2.0$ ΔR between jets > 0.75

TABLE I. Summary of event selection requirements for different stages of this analysis. The top panel includes the inclusive Z selection cuts used for determining the electron energy scale shift. The middle panel contains the additional cuts for a $Z + 1$ jet selection, used to determine the lepton scale factors in the Monte Carlo. The bottom panel contains the signal region event requirements (a $Z + 2$ jet selection).

4. WW production. This is indistinguishable from the signal in the non-btagged region. This background is evaluated using a Monte Carlo calculation.

A full list of background estimates is shown in Tab. II.

We use data corresponding to an integrated luminosity of 6.6 fb^{-1} . All data must be certified good for calorimeter, inner tracking (silicon) detectors, and the muon detectors. Background estimates are derived from Monte Carlo calculations using a combination of PYTHIA [3] and ALPGEN [4], with the geometric and kinematic acceptance obtained using a GEANT-based simulation of the CDF II detector [5]. We use the CTEQ61M parton distribution functions to model the momentum distribution of the initial-state partons [6].

Process	$e-e$	$\mu-\mu$	N_{events}
$Z \rightarrow e^+, e^-$	6239	0.0	6239
$Z \rightarrow \mu^+, \mu^-$	0.521	4399	4399
$Z \rightarrow \tau^+, \tau^-$	1.88	0.5071	2.38
$t\bar{t}$	5.13	3.69	8.82
WW	0.665	0.206	0.871
Fakes	320	4	324
Predicted Background	6568	4407	10975
Predicted ZW/ZZ	109	78.8	187.5
Total Predicted	6677	4486	11162.5
Data	6929	4682	11611

TABLE II. The number of events in the $Z + 2$ jet signal region. Systematic uncertainties on the MC predictions will be shown later. Overall, we see good agreement in the number of events in our $Z + 2$ jet region.

The final number of events is extracted by a fit to the di-jet invariant mass distribution. We split the data into three channels: a heavy-flavor tagged region, a light-flavor tagged region, and the rest (see Figure 1, and perform a simultaneous fit to the region $30 \text{ GeV} < M_{jj} < 200 \text{ GeV}$. We use the neural-network jet b ness value, described in [2], for the heavy-flavor tagged region. We use a neural-network quark-gluon discriminant, described in this note in Section III, to create the light-flavor tagged region. The fit is described in more detail in Section VI.

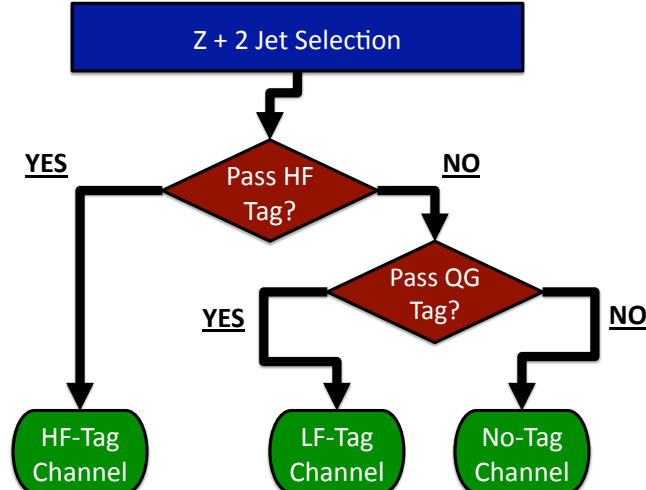


FIG. 1. Flow chart showing how the events in our $Z + 2$ jet signal region are divided into our three fitting channels. First, we use the jet b_{ness} values to tag jets likely from a $Z \rightarrow$ heavy flavor quarks decay. For events that fail that cut, we then use the jet QG values to tag jets likely from a $Z \rightarrow$ light flavor quarks decay. The remaining events enter a no-tag channel.

III. ARTIFICIAL NEURAL-NETWORK BASED QUARK/GLUON DISCRIMINANT

We are motivated to try to separate quark jets from gluon jets by the fact that the jets in our signal come entirely from the decay of W or Z bosons to quarks, while a significant part of the dominant $Z+$ jets backgrounds contains gluons. The separation is based on the fact that gluon jets tend to be more spatially spread out than quark jets. We use a neural network-based approach to quantifying the degree to which jets are spatially spread, both in deposition of their energy in the calorimeter, and in the location of tracks contained within the jet cone.

The discriminant uses three total neural networks to produce a final QG discriminant value. There are separate networks for separating quark jets and gluon jets by looking at the distribution of the distance between tower pairs inside of them, weighted by their energy content and the distance between track pairs inside of them, weighted by their momentum content (shown in Figure 2). We train a two neural networks to use these distributions to separate quark jets (“signal”) and gluon jets (“background”) from an ALPGEN $Z \rightarrow \mu^+\mu^- + 2$ partons sample. Thus, every jet is assigned a Tower NN value and a Track NN value. These two NN output values are combined with other variables to form a third neural network, whose output is the final QG discriminant. Those input variables are listed here:

- Track NN Value, evaluated by looking at the distribution of distances between pairs of tracks in a cone of $\Delta R = 0.7$ around the jet.
- Tower NN Value, evaluated by looking at the distribution of distances between pairs of calorimeter towers in a cone of $\Delta R = 0.7$ around the jet.
- Jet η
- Jet E_T
- Jet EM Fraction
- N_{vert}
- ΣE (cone 0.4) / ΣE (cone 0.7)
- ΣP (cone 0.4) / ΣP (cone 0.7)
- N_{Tracks} (cone 0.4)

- N_{Towers} (cone 0.4)
- N_{Tracks} (cone 0.7)
- N_{Towers} (cone 0.74)

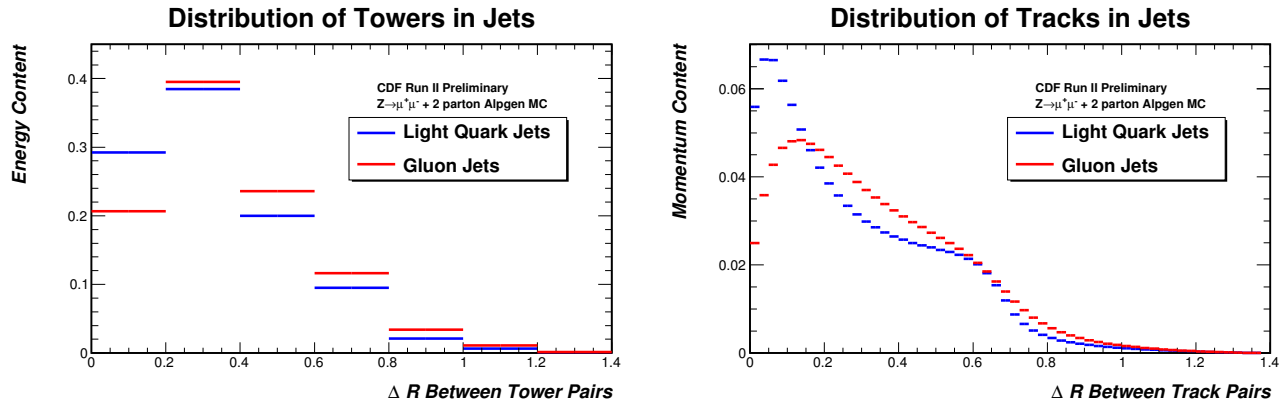


FIG. 2. The distribution of the distance between pairs of towers within a jet, with tower pairs weighted by the energy content of those pairs (left), and the distribution of the distance between pairs of tracks within a jet, with track pairs weighted by the momentum content of those pairs. It is easy to see that, overall, quark jets are more collimated than gluon jets, shown by the relative dominance of ΔR bins nearer to zero.

Figure 3 contains a flow-chart diagram showing at a basic level how these three neural networks are related. Figure 4 shows the final quark-gluon discriminant neural network training results.

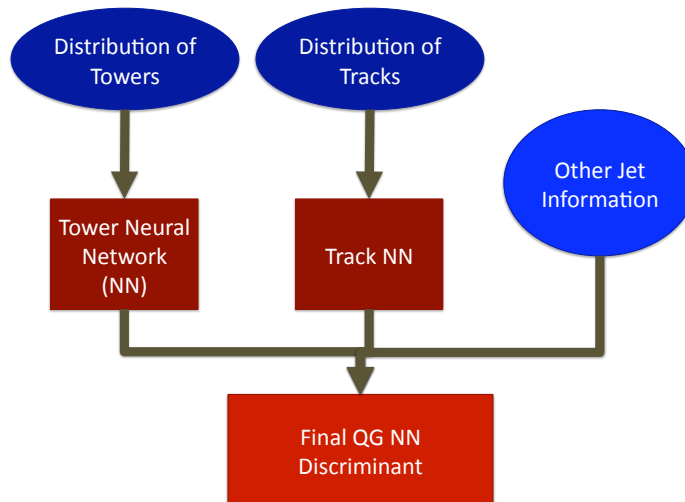


FIG. 3. Flow chart showing how the three neural networks used in our QG tagger are related.

We use a $W \rightarrow l\nu + 1$ jet selection to calibrate the response in MC of our quark-gluon discriminant. We require one high-quality electron or muon collected on high- p_T lepton triggers and $\cancel{E}_T > 25$ GeV for selecting leptonic W decays. We require high \cancel{E}_T significance (see [1, 7]), high W transverse mass ($M_T > 25$ GeV/ c^2), and place a cut on the $\Delta\phi$ between the \cancel{E}_T and other jets in order to reduce the QCD multi-jet background. These cuts are summarized in Table III. We apply a linear bin-by-bin correction function to the MC to force agreement to the data for the Track NN and Tower NN values. These corrected values are used as inputs into the final QG discriminant, and we see much

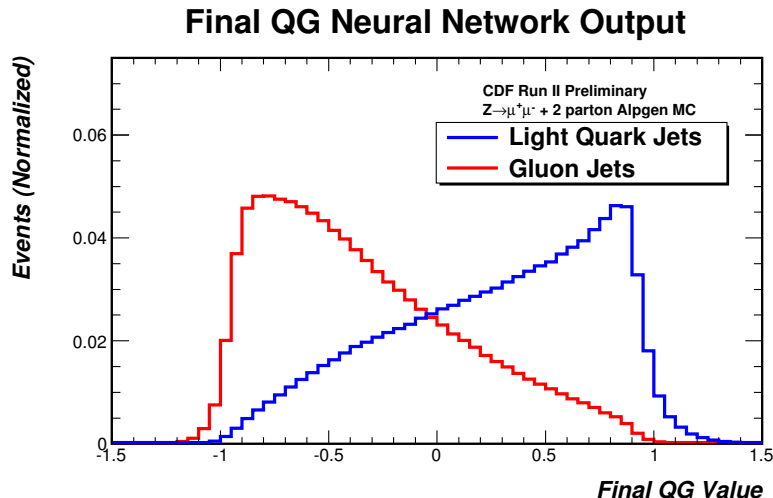


FIG. 4. The output NN distribution after the training of the NN-based quark/gluon discriminant using, separating light quark jets (signal) and gluon jets (background).

improved agreement with data in that variable, shown in Figure 5. We evaluate a systematic uncertainty based on the placement of a cut in this distribution, described in Section V.

$W \rightarrow l\nu$ Selection
$N_{vtx} > 0$
$ z_0 < 60$ cm
Lepton $p_T > 20$ GeV/ c
$\cancel{E}_T > 25$ GeV
$WM_T > 25$ GeV
\cancel{E}_T -sig > 1 for muon events, > 4 for electron events
$\Delta\phi$ between \cancel{E}_T and jet ($E_T > 5$ GeV) > 0.2
$W + 1$ jet
N_{jets} with $E_T > 20$ GeV = 1
Jet $E_T > 20$ GeV, $ \eta < 2.0$
$W + 2$ jets
N_{jets} with $E_T > 20$ GeV = 2
Jet $E'_T > 20$ GeV, $ \eta 's < 2.0$

TABLE III. Summary of event selection requirements for our $W + 1/2$ jet selection, used to calibrate parts of our QG discriminant.

IV. $Z + 1$ JET BALANCING

We can investigate the modeling of jet energies by looking at the balancing of a jet and Z boson. In events with only one jet, low \cancel{E}_T , and a well-reconstructed $Z \rightarrow l^+l^-$ decay, the jet and Z boson's transverse momenta should be well balanced. Looking at this Z -jet balancing gives us a check on the jet energy scale for jets as a function of any desired jet variable.

Our selection for the Z -jet balancing studies is very similar to the $Z + 1$ jet selection we use for determining our MC lepton-pair scale factors. The basic selection cuts are listed in Table I. We additionally require that there are no other jets with E_T above 3 GeV in the event, and that the Z P_T is above 30 GeV/ c , in order to avoid any threshold effects with our selected 20 GeV jet energy cut.

Figure 6 shows the Z -jet balancing as a function of the jet QG value. It appears as though the modeling from MC

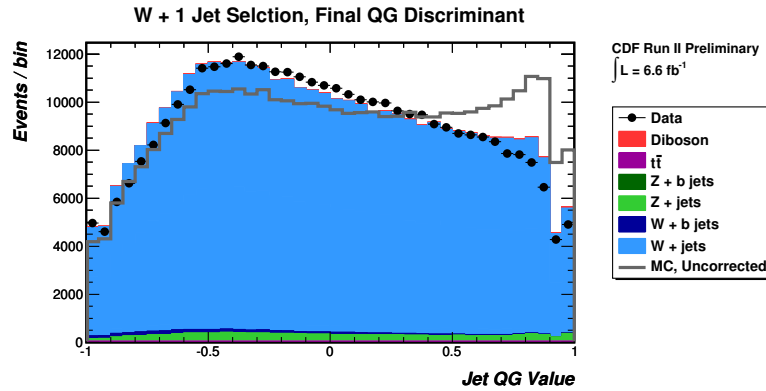


FIG. 5. The distribution of the final QG neural network values in our $W + 1$ jet selection. We show the MC distribution before and after the corrections to the Tower and Track NN values; we see, not surprisingly, much better agreement between data and MC after the corrections are applied. Overall the data MC models the data fairly well, though we will need to introduce a systematic uncertainty for placing a cut on the QG values of the jets.

is good for high-QG (more collimated, and more quark-like), but poor for low-QG jets (more spread out and more gluon-like). We find that shifting the jet energy scale (JES) for gluons by 2σ provides rather good agreement, while other JES shifting schemes do not. Thus, throughout the analysis, we shift gluon JES values down by 2σ . Figure 7 show the Z -jet balancing as a function of the jet η and E_T .

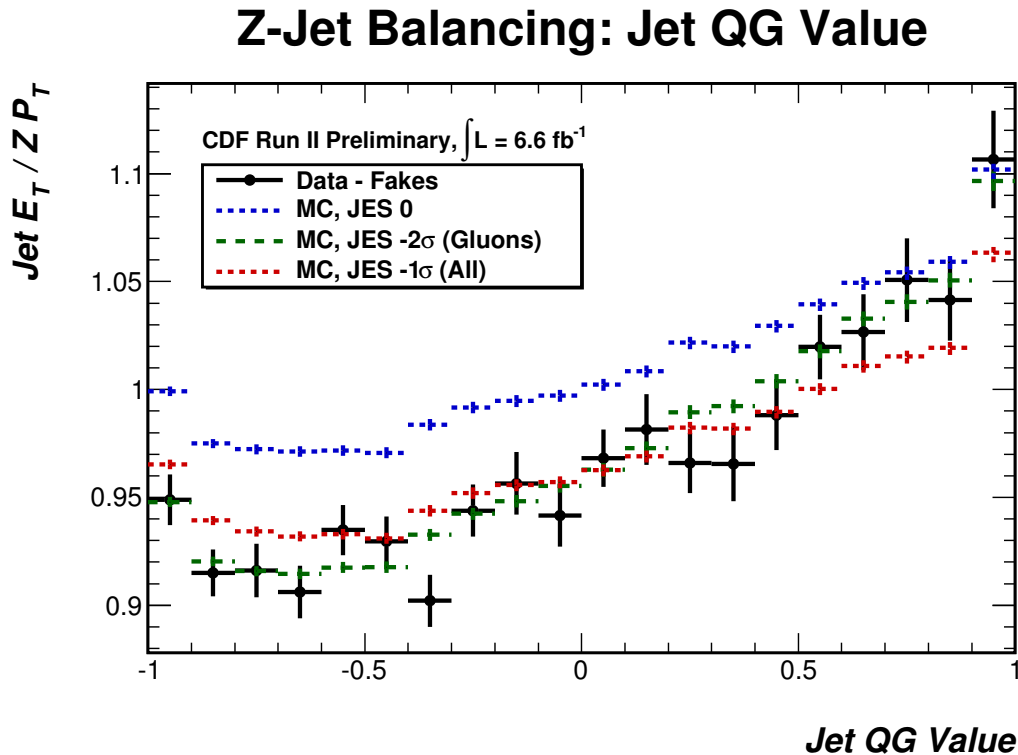


FIG. 6. Profile histogram showing the Z -jet transverse momentum balancing as a function of the QG value of the jet. Higher QG values correspond to more quark-like jets. Thus, we see rather good agreement for quark-like jets, while poor agreement between data and MC for gluon-like jets.

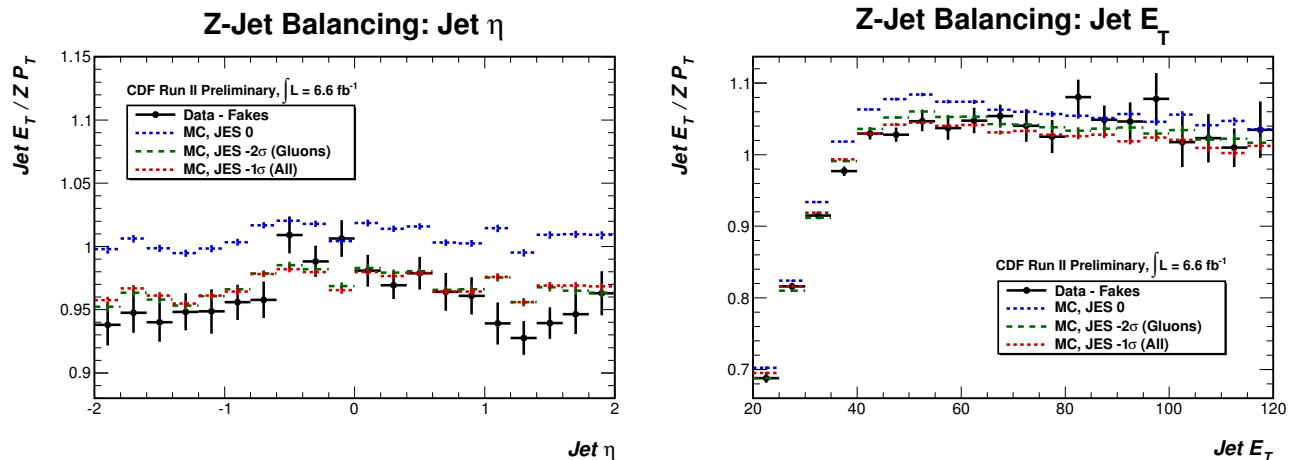


FIG. 7. Profile histogram showing the Z -jet transverse momentum balancing as a function of the jet η (left) and E_T (right). We see a strange behavior where central jets are more accurately modeled by the MC than more forward jets. While we see good agreement for high- E_T jets (though we are limited by small sample size of the data here), we see much poorer agreement for low jet E_T , indicating we need to somehow correct the MC.

V. EVALUATION OF TAGGING EFFICIENCY

To perform our tagging, we use the jet b_{ness} and jet QG values of the two jets in our signal region events. We combine the neural network values for the two jets into a single quantity. Since both the b_{ness} and QG neural networks use hyperbolic tangent as a response function, we take the inverse hyperbolic tangent of each jet's b_{ness} (or QG) value, sum them, and then take hyperbolic tangent of that sum. So, if b_1 is the first jet's b_{ness} , and b_2 is the second jet's b_{ness} , the variable we tag on is:

$$b_{\text{Sum}} = \tanh(\operatorname{atanh}(b_1) + \operatorname{atanh}(b_2)).$$

We do a similar thing for the Jet QG values. These “sum” b_{ness} and QG distributions are shown in Figures 8 and 9. We determine that an optimal cut for determining the channels in our fit to data is the following:

- Heavy-flavor tagged channel: Events with Sum $b_{\text{ness}} > 0.0$.
- Light-flavor tagged channel: Events with Sum $b_{\text{ness}} < 0.0$ and with Sum QG > 0.0 .
- No-tag channel: Events with Sum $b_{\text{ness}} < 0.0$ and with Sum QG < 0.0 .

We use comparisons of data and MC in a $t\bar{t}$ dilepton sample to determine the tagging efficiency of our Sum b_{ness} cut, and use a comparison in $W + 2$ jets to determine the mistag rate of that cut. The $t\bar{t}$ dilepton selection is almost identical to the $Z + 2$ jets in Table I, but with a dilepton mass outside of the Z window ($M_{ll} < 76 \text{ GeV}/c^2$ or $M_{ll} > 106 \text{ GeV}/c^2$), and $\cancel{E}_T > 40 \text{ GeV}$; the $W + 2$ jet selection is in Table III. We correct the MC to match the tagging efficiency (or mistag rate) in the data by changing the Sum b_{ness} cut in MC to match that of data. We apply an uncertainty to this correction in a similar manner. The distributions of the Sum b_{ness} in these two samples are shown in Figure 10, and the tagging efficiency and mistag rate for the Sum b_{ness} cut are summarized in Table IV.

Data	MC	Equivalent MC Cuts ($-1\sigma, 0, +1\sigma$)
$m_D = 0.0557 \pm 0.0036$	$m_{MC} = 0.04111$	$(-0.27, -0.24, -0.18)$
$e_D = 0.580 \pm 0.056$	$e_{MC} = 0.6574$	$(+0.1, +0.35, +0.6)$

TABLE IV. The efficiency and mistag rates for our b_{ness} cut evaluated in data and MC, along with the necessary cut value changes in MC to model the proper rates and the uncertainties on them.

We follow a similar procedure to determine the tagging efficiency of our Sum QG cuts. We determine the tagging efficiency for our signal from a $t\bar{t} \rightarrow l\nu q\bar{q}'b\bar{b}$ lepton + jets sample, where we select the quark jets from the decay of

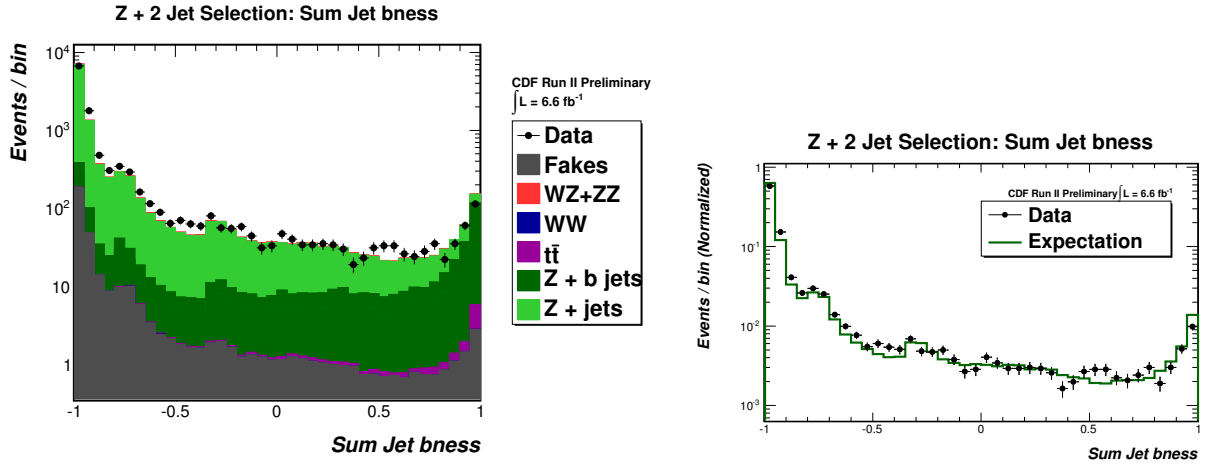


FIG. 8. The distribution of the “sum” of jet $bness$ in our $Z + 2$ jet region. Overall we see pretty good agreement in data and MC, and we see MC samples with b -quarks in them ($t\bar{t}$ and $Z + b\bar{b}$) show high values, as expected.

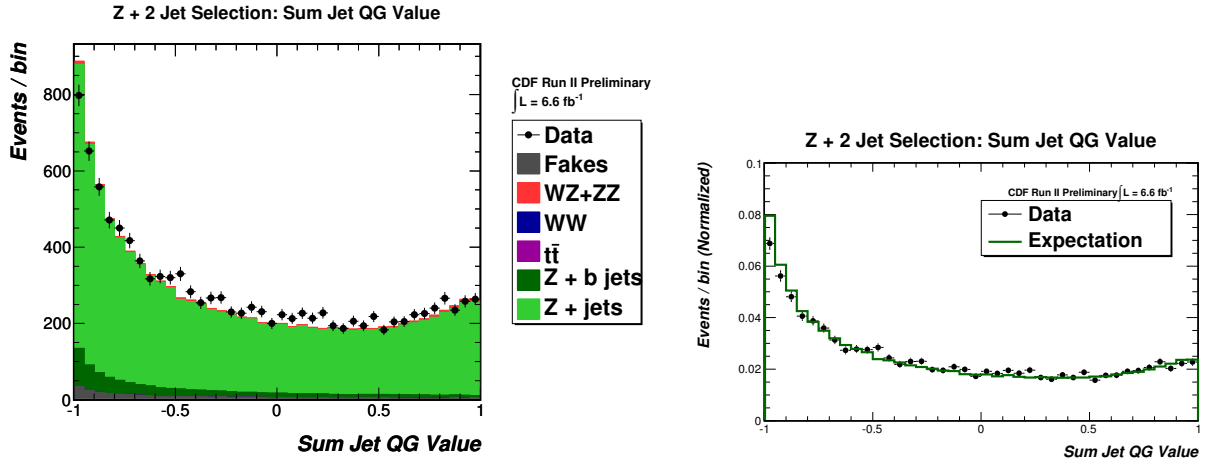


FIG. 9. The distribution of the “sum” of jet QG values in our $Z + 2$ jet region. Overall we see pretty good agreement in data and MC. Our diboson sample is pretty much flat across this distribution, while our $Z +$ jets background tends to peak at low QG values (there are many events with a significant gluon component).

a W boson by first removing the jets that look most like b 's. We determine the tagging efficiency for our dominant $Z +$ jets background by comparing data and MC in a $W + 2$ jet region. We correct the MC to match the tagging efficiencies in data by changing the Sum QG cut to match the efficiency of the data, applying an uncertainty to this correction in a similar manner. The distributions of the Sum QG in these two samples are shown in Figure ??, and the tagging efficiencies are summarized in Table V.

Data	MC	Equivalent MC Cuts ($-1\sigma, 0, +1\sigma$)	Sample Applied To
$e_{D,t\bar{t}} = 0.401 \pm 0.030$	$e_{MC} = 0.436$	(+0.00, +0.09, +0.18)	Signal
$e_{D,Vjj} = 0.396 \pm 0.009$	$e_{MC} = 0.393$	(-0.03, -0.01, +0.00)	$Z +$ jets

TABLE V. The efficiency and mistag rates for our QG cut evaluated in data and MC, along with the necessary cut value changes in MC to model the proper rates and the uncertainties on them.

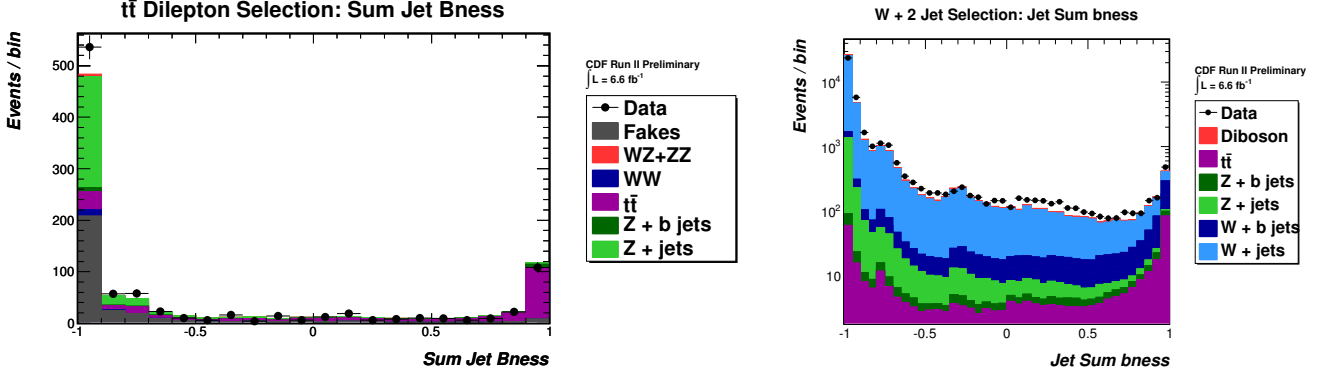


FIG. 10. (Left) The distribution of the “sum” of jet $bness$ in our $t\bar{t}$ dilepton sample, from which we evaluate a tag efficiency scale factor for MC. (Right) The distribution of the “sum” of jet $bness$ in our $W + 2$ jets sample, from which we evaluate a mistag rate scale factor for the MC.

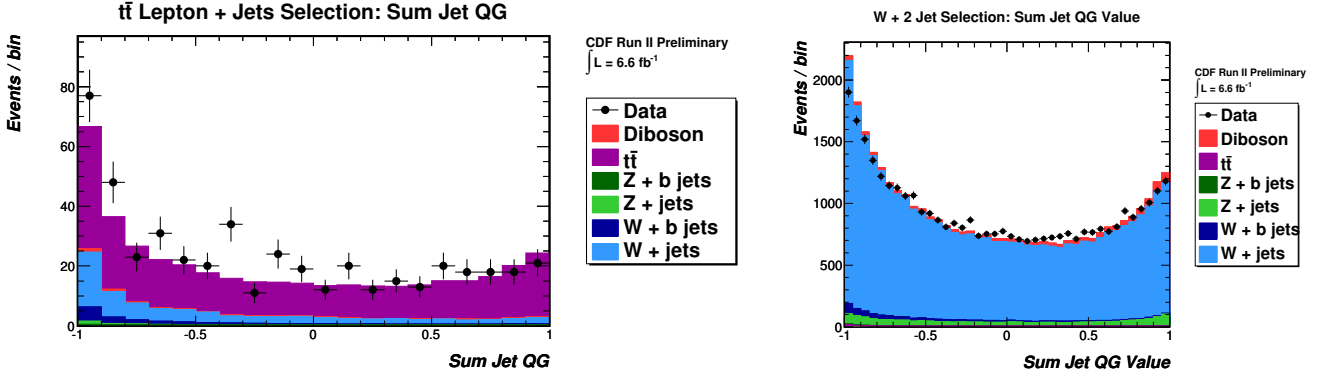


FIG. 11. The distribution of the “sum” of jet QG in our $t\bar{t}$ lepton + jets sample (left) and our $W + 2$ jets sample (right).

VI. SIGNAL EXTRACTION AND RESULTS

The signal extraction is performed by fitting the dijet mass distribution between $30 \text{ GeV}/c^2$ and $200 \text{ GeV}/c^2$ (using 17 bins of bin width $10 \text{ GeV}/c^2$) in three different channels: a heavy-flavor tagged region, a light-flavor tagged region, and a no-tag region. To perform the fit, we use the `mclimit` package [10]. The data is fit to the following templates:

- **$Z + \text{jets}$ background (EWK):** Our largest background, we allow the $Z + \text{jets}$ background normalization to float unconstrained and independently in the three different channels, allowing us to avoid uncertainties due to the relative fraction of heavy flavor jets, quark jets, and gluon jets in the various channels.
- **$t\bar{t}$ (TOP):** We constrain the $t\bar{t}$ normalization to its measured cross section with an uncertainty of 6%.
- **WW:** We also constrain the WW normalization to its measured cross section with an uncertainty of 6%.
- **Fakes:** We constrain the normalization on the fakes to $\pm 25\%$. As this is a data-driven background template, no other uncertainties are applied to it.
- **ZW/ZZ (SIG):** Our signal’s normalization is allowed to float unconstrained in the fit, but unlike the $Z + \text{jets}$ background, not independently between channels.

The number of events from each template in each channel is given in Table VI, and the dijet mass distributions are shown in Figures 12-14.

In performing the fit, we simultaneously fit for the following systematic errors:

Process	N_{events} (HF Tag)	N_{events} (LF Tag)	N_{events} (No Tag)
$Z + jets$	730 ± 120	3510^{+550}_{-630}	5490^{+970}_{-1120}
$t\bar{t}$	$4.26^{+0.56}_{-0.59}$	$0.86^{+0.23}_{-0.27}$	$2.51^{+0.42}_{-0.36}$
WW	0.025 ± 0.002	$0.26^{+0.07}_{-0.04}$	$0.56^{+0.19}_{-0.19}$
Fakes	18.9 ± 4.7	82 ± 21	196 ± 49
Total Background	760^{+120}_{-130}	3600^{+550}_{-620}	5690^{+970}_{-1120}
WZ/ZZ	$15.9^{+2.0}_{-2.1}$	$87.2^{+9.7}_{-9.4}$	$80.3^{+9.6}_{-9.2}$
Total Predicted	770^{+120}_{-130}	3690^{+560}_{-630}	5770^{+980}_{-1120}
Data	685 ± 26	3942 ± 63	5976 ± 77

TABLE VI. The number of events in each channel of the fit of the dijet mass distribution. Uncertainties are not provided for the EWK and SIG samples, as they are allowed to float in the fits in mclimit.

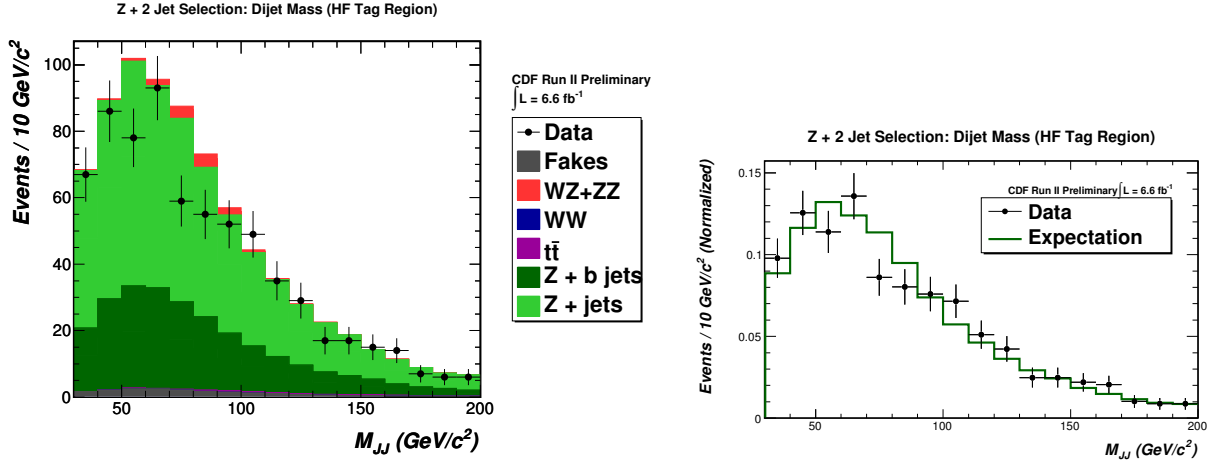


FIG. 12. The dijet mass distribution in our heavy-flavor-tagged channel, with MC normalized absolutely (left) and to equal area with the data (right).

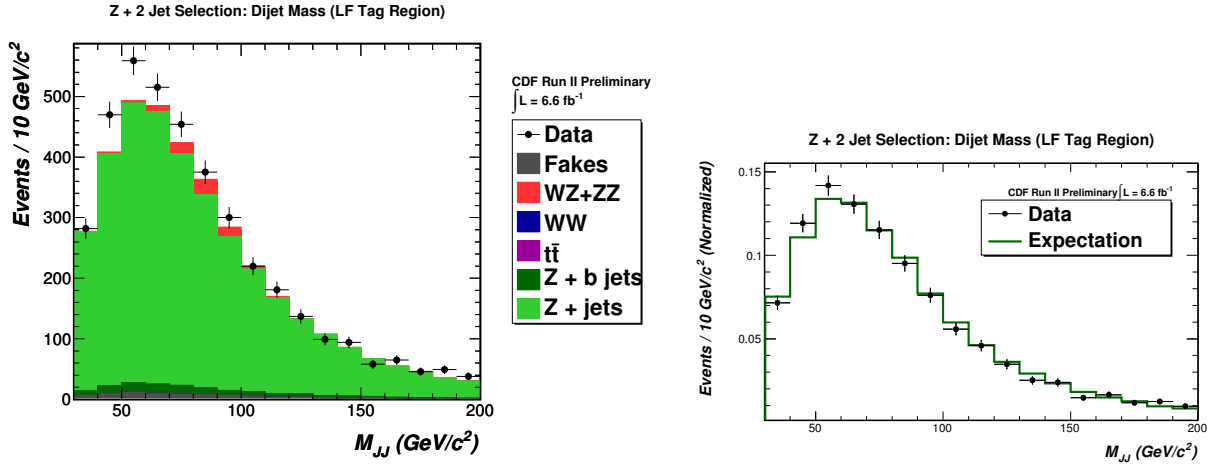


FIG. 13. The dijet mass distribution in our light-flavor-tagged channel, with MC normalized absolutely (left) and to equal area with the data (right).

- **Jet Energy Scale (JES):** We raise and lower the JES by $\pm 1\sigma$, obtaining templates reflecting both a change in the number of events and different background and signal shapes.

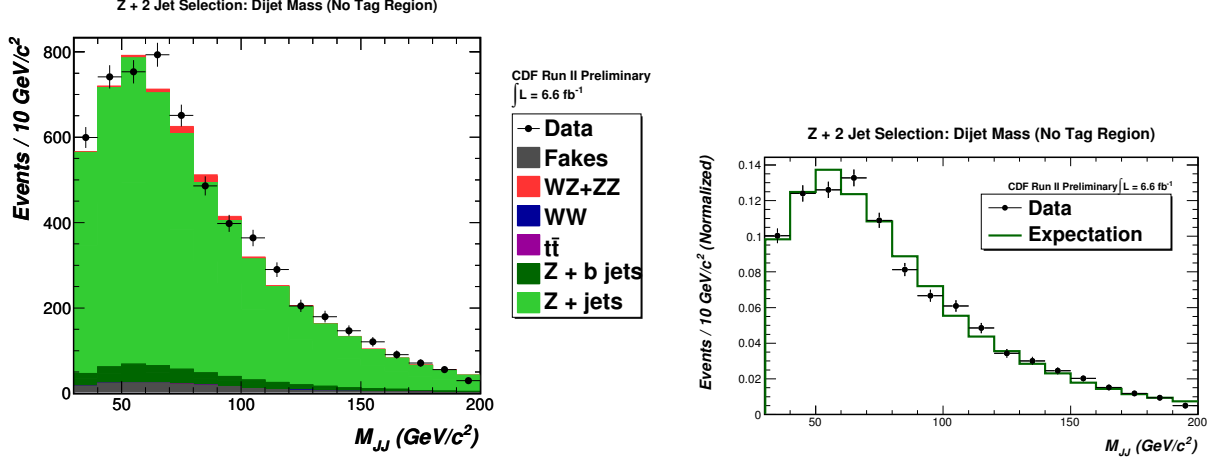


FIG. 14. The dijet mass distribution in our no-tag channel, with MC normalized absolutely (left) and to equal area with the data (right).

- **bness Cut (BNS):** We raise and lower the *bness* cuts in MC according, as described in Section V.
- **QG Discriminant Cut (QG):** Similarly, we raise and lower the QG cuts in MC according, as described in Section V.
- **Q^2 (Q2):** We use higher and lower Q^2 MC samples to evaluate a shape only systematic for the EWK background template.

These systematic uncertainties (and the uncertainties on the normalizations of the background templates) are summarized in Table VII.

	Normalization	JES	<i>b</i> -tag	QG-Tag	Q^2
<i>Z</i> + jets					
<i>HF Tag Region</i>	—	±12%	+10%, -8.3%	—	Shape Only
<i>LF Tag Region</i>	—	+14%, -16%	-0.5%, +0.4%	+1.0%, -1.9%	Shape Only
<i>No Tag Region</i>	—	+16%, -19%	-1.0%, +0.9%	-0.6%, 1.2%	Shape Only
<i>t</i> \bar{t}					
<i>HF Tag Region</i>	±6.45%	+0.4%, -0.1%	+8.9%, -9.8%	—	—
<i>LF Tag Region</i>	±6.45%	+0.3%, -0.4%	-17%, +16%	+11%, -19%	—
<i>No Tag Region</i>	±6.45%	+4.4%, -2.4%	-9.5%, +11%	-3.8%, 6.6%	—
<i>WW</i>					
<i>HF Tag Region</i>	±6%	—	—	—	—
<i>LF Tag Region</i>	±6%	+12%, -9.4%	—	+20%, -0%	—
<i>No Tag Region</i>	±6%	+32%, -8.4%	—	-9.6%, -0%	—
Signal					
<i>HF Tag Region</i>	—	+4.2%, -4.3%	+9.7%, -10%	—	—
<i>LF Tag Region</i>	—	+5.5%, -4.4%	-0.7%, +0.6%	+6.3%, -6.6%	—
<i>No Tag Region</i>	—	+6.0%, -5.4%	-1.2%, +1.4%	-6.9%, +7.2%	—
Fakes (All Regions)	±25%	—	—	—	—

TABLE VII. The systematic uncertainties that are included as nuisance parameters in the fit to the data.

In addition, we consider the following acceptance uncertainties:

- **Jet Resolution:** Smearing the jet energies produces an overall normalization difference of 2.5%.
- **Lepton Trigger/Reconstruction Efficiencies:** We assign a 2.2% uncertainty based on the trigger and reconstruction efficiencies we calculate by comparing data and MC in the *Z* + 1 jet region.

- **Lepton Energy Scale:** Raising and lowering the LES of all leptons by $\pm 1\%$, has a slight effect on the acceptance (0.65%).
- **Lepton Energy Resolution:** Smearing all lepton energy/momenta using a Gaussian distribution with a width of 2% of the lepton's energy can give a normalization uncertainty of 0.14%.
- **Initial/Final State Radiation:** We take the uncertainty of 1.2% calculated from changing the amount of initial and final state radiation in our MC samples.
- **PDF:** We take a 2% uncertainty due to differences in the PDFs (see [2]).
- **Luminosity:** We take a 6% uncertainty on the integrated luminosity of our analyzed data.

The results of the fit to the data are shown in Table VIII. We fit for no signal events in our data. This is also seen in the stack plots of the fits to data, shown in Figure 15.

Process	N_{events} (HF Tag)	N_{events} (LF Tag)	N_{events} (No Tag)
$Z + jets$	660^{+170}_{-150}	3900^{+920}_{-800}	5800^{+1300}_{-1800}
$t\bar{t}$	$4.26^{+0.56}_{-0.59}$	$0.86^{+0.19}_{-0.23}$	$2.51^{+0.42}_{-0.36}$
WW	0.025 ± 0.002	$0.26^{+0.07}_{-0.04}$	$0.56^{+0.07}_{-0.19}$
Fakes	18.3 ± 4.7	80 ± 21	190 ± 49
WZ/ZZ	$0^{+3.3}_{at\ limit}$	$0^{+17}_{at\ limit}$	$0^{+16}_{at\ limit}$
Data	685 ± 26	3942 ± 63	5976 ± 77

TABLE VIII. The result of the fit from mclimit. We fit for no signal in our data, as can be seen in the final shapes of the templates in Figure 15.

To translate the result of our fit to the data to bounds or limits on the true cross section of $WZ+ZZ$ production, we construct Feldman-Cousins bands by analyzing the distribution of fitted (*i.e.*, measured) cross sections in pseudo-experiments generated with a variety of scale factors on the input signal cross section. The set of input cross sections in our pseudo-experiments range from 0.1 to 4.0 times the standard model value with a step size of 0.1.

Figure 16 shows the results of our Feldman-Cousins analysis in our 3-channel fit. The return of the fits, if they are to be believed, allow us to set a limit on $\sigma_{measured}$ at about $1.3 \times \sigma_{SM}$ with 95% CL. Using $\sigma_{SM} = \sigma_{WZ} + \sigma_{ZZ} = 5.08$ pb, we then calculate $\sigma_{measured} < 6.6$ pb at 95% CL. The expected limit was $2.3 \times \sigma_{SM}$.

ACKNOWLEDGMENTS

We thank the Fermilab staff and the technical staffs of the participating institutions for their vital contributions. This work was supported by the U.S. Department of Energy and National Science Foundation; the Italian Istituto Nazionale di Fisica Nucleare; the Ministry of Education, Culture, Sports, Science and Technology of Japan; the Natural Sciences and Engineering Research Council of Canada; the National Science Council of the Republic of China; the Swiss National Science Foundation; the A.P. Sloan Foundation; the Bundesministerium für Bildung und Forschung, Germany; the World Class University Program, the National Research Foundation of Korea; the Science and Technology Facilities Council and the Royal Society, UK; the Institut National de Physique Nucleaire et Physique des Particules/CNRS; the Russian Foundation for Basic Research; the Ministerio de Ciencia e Innovación, and Programa Consolider-Ingenio 2010, Spain; the Slovak R&D Agency; and the Academy of Finland.

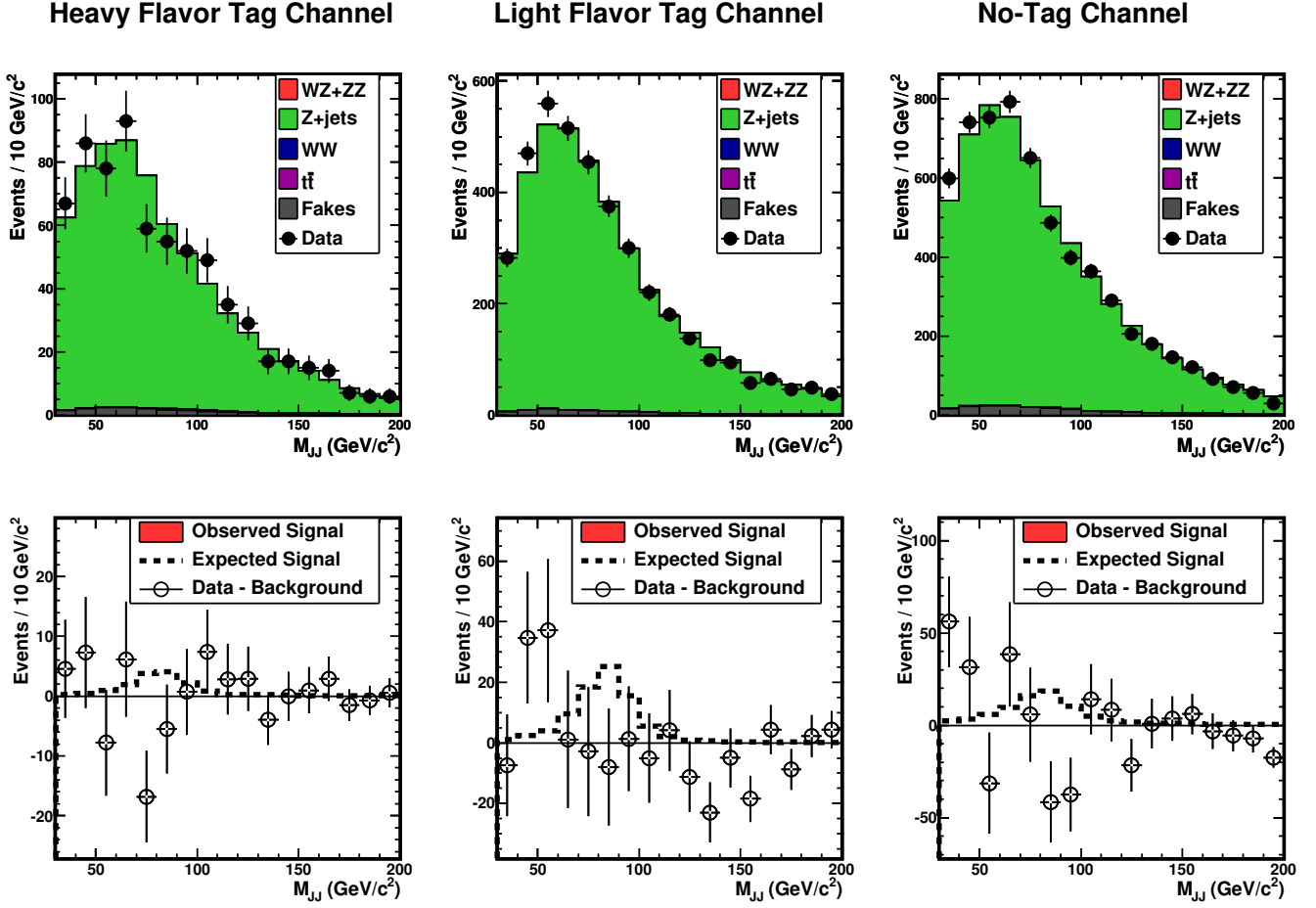
CDF Run II Preliminary, $\int L = 6.6 \text{ fb}^{-1}$ 

FIG. 15. Result of the fit from mclimit. The top row shows the fits to the input templates (with signal), and the bottom row shows the difference plot of the data and the background, along with the signal fit. Since we fit for no signal, there is no signal visible in the final row of plots.

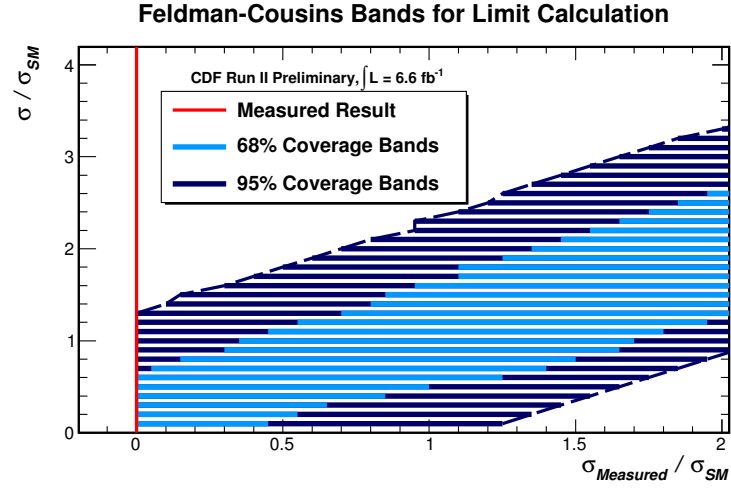


FIG. 16. Feldman-Cousins bands for the dijet mass fit, showing the expected range of measured cross sections as a function of the true cross section, with 68% CL (light blue) and 95% CL (dark blue). Our measured result points towards a limit of $1.3 \times \sigma_{SM}$ with 95% CL, while we would have expected to set a limit of $2.3 \times \sigma_{SM}$.

-
- [1] T. Aaltonen *et al.* (CDF Collaboration), Phys. Rev. Lett. **103**, 091803 (2009), arXiv:0905.4714.
 - [2] Search for WZ/ZZ in $\cancel{E}_T + b\bar{b}$ channel, CDF note CDF/ANAL/ELECTROWEAK/CDFR/10311 (2010), http://www-cdf.fnal.gov/cdfnotes/cdf10311_metbb_pubnote.pdf.
 - [3] T. Sjöstrand *et al.*, J. High Energy Phys. **0605**, 026 (2006).
 - [4] M. L. Mangano *et al.*, J. High Energy Phys. **07**, 001 (2003).
 - [5] R. Brun *et al.*, CERN Report No. CERN-DD-78-2-REV (unpublished).
 - [6] J. Pumplin *et al.*, J. High Energy Phys. **0207**, 012 (2002).
 - [7] M. Goncharov *et al.*, Nucl. Instrum. Methods Phys. Res., Sect. A **565**, 543 (2006).
 - [8] T. Aaltonen *et al.*, Phys. Rev. D **79**, 052008 (2009).
 - [9] T. Aaltonen *et al.* (CDF Collaboration), Phys. Rev. **D** 79, 052007 (2009).
 - [10] T. Junk, Nucl. Instrum. Meth. **A** 434:435-443 (1999), arXiv:hep-ex/9902006v1.
 - [11] Gary J. Feldman and Robert D. Cousins, Phys. Rev. D **57**, 3873 (1998).